

Results on Total and Elastic Cross Sections in Proton–Proton Collisions at $\sqrt{s} = 200 \text{ GeV}$

Abstract

We report the results on the total and elastic cross sections in proton-proton collisions at $\sqrt{s} = 200 \text{ GeV}$. The results were obtained with the Roman Pot setup of the STAR experiment at the Relativistic Heavy Ion Collider (RHIC). The setup was used to measure elastic differential cross section in the four-momentum transfer squared (t) range $0.045 \leq -t \leq 0.14 \text{ (GeV/c)}^2$. The results include the value of the exponential slope parameter B of the elastic differential cross section $d\sigma/dt$ in the measured small $-t$ range and the total cross section σ_{tot} obtained from the extrapolation of the $d\sigma/dt$ to the optical point at $-t = 0 \text{ (GeV/c)}^2$. We also present the value of elastic cross section σ_{el} . All results are compared with the world data.

Keywords: Elastic Scattering, Diffraction

5 1. Introduction

The elastic scattering plays a special role in proton–proton (pp) scattering at high energies, which is evident by the fact that it contributes almost 20% of the total cross section at the highest energies where it was measured. The highest center of mass energy (\sqrt{s}) at which the pp elastic and total cross sections have
10 been measured at the accelerators has been achieved at the LHC in the range of $2.76 \leq \sqrt{s} \leq 13 \text{ TeV}$ [?]. Below the LHC’s \sqrt{s} the highest energy results are for the Intersecting Storage Rings (ISR) at $\sqrt{s} = 62.4 \text{ GeV}$. It is important to have measurements in the energy gap between the ISR and the LHC to constrain the phenomenological models of the pp cross sections. There are also new features
15 of the elastic cross section $d\sigma_{el}/dt$ observed at the LHC, which were not seen

at the ISR. For example it was observed at the LHC at $\sqrt{s} = 8$ TeV the elastic the exponential shape $\exp(-Bt)$ of the elastic cross section as function of the four momentum transferred squared (t) has a quadratic term in t , something that was not observed at the ISR. A possibility of this non-linear behavior can also be checked at RHIC energies. Another important need to know those pp cross sections in RHIC energy range is because at that range one still expects a difference between pp and proton-antiproton $p\bar{p}$ cross sections, which were measured up to 1.8 TeV. Such difference affects fits to the phenomenological models [1]

2. The Experiment

The results presented here were obtained by the STAR experiment with the Roman Pot (RP) setup. The main part of the setup is the RP system of the pp2pp experiment [2] used to detect scattered forward protons. The RP system was installed downstream of the STAR detector at RHIC, see Fig. 1, where the location of the Roman Pots, top view, and schematically four Si detectors and a trigger scintillation counter package in each Roman Pots are shown. The four planes of Si strip detectors, two measuring x-coordinate and two measuring y-coordinate, are used to reconstruct position of the proton at the RP. The scintillation counter in each RP was used for triggering on the candidate events with forward protons. The location between DX and D0 RHIC dipole magnets is such that no special accelerator conditions, like large β^* and parallel to point focusing are needed to operate Roman Pots together with the rest of the STAR experiment's physics program. As a consequence the STAR physics program now includes, in addition to elastic scattering, other measurements that require detection of forward protons: a) Central Exclusive Production (CEP) [3] and b) particle production in both Single Diffraction Dissociation (SDD) and Central Diffraction [4]. In those inelastic events STAR detector is used to characterize the recoil system at central rapidity.

The DX magnet and the two Roman Pot detectors allow measurement of

45 momentum vector of the scattered protons at the detection point. Using the known bending angle of the DX magnet, one can determine the scattering angle in the (x,z) plane θ_x . The scattering angle in the (y,z) plane θ_y is determined from the y-coordinate measured in the RPs.

The data were acquired with no special RHIC running conditions with normal $\beta^* = 0.85m$. In addition we had: a) Fur hours at the end of a store to have
50 cleanest beam possible; b) Three special luminosity measurements to minimize systematic uncertainty on luminosity measurement; and c) Move Roman Pots as close as possible, they were moved closer than during nominal data taking. Luminosity was $\approx 45 \cdot 10^{30} cm^{-2} sec^{-1}$. There were about 6.7 Million triggers
55 collected for the integrated luminosity $1.8pb^{-1}$. The achieved closest distance of the first readout strip was about 30 mm or about $10\sigma_y$ of the beam, which corresponds minimum four-momentum transfer $|t_{min}| \approx 0.03 GeV/c^2$.

3. Alignment and Track Reconstruction

Here we discuss three steps needed for track reconstruction in Si detectors:
60 clustering that is used to determine position of the proton trajectory in the Si plane, alignment to obtain the position of the proton in the elastic scattering coordinate system and the reconstruction of tracks, which leads to the reconstruction of scattering angle needed to determine the t -value.

3.1. Clustering

65 To reconstruct track points in the RPs we start with a clustering procedure, which is used for each Si detector plane separately. In the first step the noise cut of energy bigger than $3\sigma_{RMS}$ above the pedestal is applied for each strip. The procedure searches for the channel with maximum signal and continuous series of channels adjacent to it - the chain of channels found this way, called cluster,
70 is removed from the pool of hits in a given plane and procedure is repeated until there are no more hits in the plane. The energy distribution of reconstructed clusters is in good agreement with convoluted Landau and Gauss distributions, as expected, see Fig. ??.

Positions of clusters found in both X or Y planes were compared and a pair
75 of clusters for a given coordinate was accepted as a point in x or y -coordinate
if their positions difference $\Delta_{x,y}$ satisfied condition $\Delta_{x,y} \leq 2 \cdot d_{strip} \approx 200 \mu m$,
where d_{strip} is strip pitch. Pairs of matched clusters found in detector planes
measuring the same coordinate define (x, y) coordinates of space points for given
RP. In most of the events, $\sim 95\%$, only one reconstructed space point in an RP
80 was found. Position of the point is calculated as an average of the matched
cluster positions.

3.2. Alignment

Before the reconstruction of the scattering angle an alignment procedure
was performed in two steps, each producing one set of offsets. In the first
85 step survey data are utilized. In the first step, the survey was done by the
survey group of the accelerator department after the installation of the detector
packages in the Roman Pots. This survey determined (x,y) position of the
first strip in each detector package with respect to the accelerator coordinate
system. In the second step corrections to the survey alignment were obtained
90 using reconstructed elastic events and the condition of collinearity of elastic
scattering for tracks reconstructed on each side of the IP. For this purpose only
events with 2PT tracks on both sides of IP were used, it was also required that
these 2PT tracks are uniquely reconstructed - one and only one reconstructed
point in each RP - to assure the sample consists of cleanest elastic events.

95 For each event a least squares (LSQ) line fit was done through four recon-
structed points. For these events, mean value of residuals for each RP station
average distance of reconstructed point from fitted line was calculated. Mean
residuals found this way were applied to correct first strip position in each silicon
detector plane, and alignment process was then repeated with new strip posi-
100 tions. Typically three iterations were needed to achieve residuals distributions
centered at zero - optimal relative positions between Roman Pots on opposite
sides of in each detector arm separately. By its construction the result of the
second alignment step are set of offsets in the coordinate system of the elastic

scattering, where two outgoing protons are collinear.

105 The procedure was performed for each run used in analysis and mean value of per run corrections was applied for each detector plane.

, a mean global correction accounting for uncertainty of detector positioning and non-scattered beam trajectory - was calculated and applied in the point/track reconstruction.????

110 This procedure leaves one variable unknown: the unscattered beam trajectory in the above coordinate system, which affects the t -scale of the differential distribution dN/dt . The procedure to estimate of the beam tilt angle is described in section ??, where Monte Carlo corrections are described.

3.3. Scattering Angle Reconstruction

115 For small scattering angles θ , which are of the order of few milliadians, track-point x_{RP} and y_{RP} positions reconstructed at given RP station can be expressed as:

$$x_{RP} = x_{IP} + \theta_x(z_{RP} - z_{IP}) \quad y_{RP} = y_{IP} + \theta_y(z_{RP} - z_{IP}) \quad (1)$$

where (x_{IP}, y_{IP}, z_{IP}) are (x, y, z) positions of the primary vertex, z_{RP} is surveyed z -position of the RP station, and θ_x, θ_y are the scattering angles. Since 120 the position of primary vertex is not known on event by event basis, two reconstructed points are required to calculate the scattering angle. A track is combination of two points reconstructed in two detector stations on the same side of Interaction Point (**IP**).

4. Data Analysis

125 The data analysis has three major steps. First, from the hits in Si detectors space points are reconstructed. Second, from the space points scattering angles θ_x in (x,z) plane and θ_y in (y,z) plane are calculated. The former and the latter described in previous section. Third, cuts are applied to select elastic scattering events to extract total and elastic cross sections, which is described 130 in this section.

Given that the trigger condition was very inclusive, requiring at least one valid signal in at least one PMT on each side of the IP, the collected data sample included in addition to elastic events the contributions from background, which consisted non elastic events and accidental coincidences of the beam halo. A series of cuts was then used to select elastic events form the collected data sample. The general idea was to use two types of conditions in order to minimize the previously mentioned background: 1) Given the definition of elastic events a collinearity condition in $(\theta_{West}, \theta_{East})$ space is required, where $(\theta_{West}, \theta_{East})$ are reconstructed scattering angles on each side of the IP; 2) Choice of the fiducial volume in $(\phi, |t|)$ space, to stay within clear aperture and away from the beam halo. The following cuts were used in selection of elastic events: 1) Choose elastic event candidates by checking the hit pattern on the East and West detectors to make sure it corresponds to the elastic condition. Only events with elastic combination of reconstructed points in the the Roman Pots are accepted. Namely, combinations $(ED \wedge WU)$ or $(EU \wedge WD)$. 2) Only events with two point tracks on the East and two point tracks on the West (one track point per Roman Pot in elastic combination) were kept. 3) Since the elastic events must satisfy collinearity condition collinearity within $2\sigma_\theta$ namely $\theta_{West} - \theta_{East} < 2\sigma_\theta$, where $\sigma_\theta = 255\mu rad$, consistent with the beam angular divergence, was required. 4) Finally, events within fiducial volume in $(\phi, |t|)$ space are chosen.

In Fig. 2 we show collinearity condition $\Delta\Theta_y$ vs $\Delta\Theta_x$ with the contours of $2\sigma_\Theta$ and $3\sigma_\Theta$. It is clear that the collinearity is very well satisfied for the two-point tracks.

5. Simulation

Response of the detector was studied with GEANT4 based software package. The simulation had detailed implementation of the beam-line and Roman Pot detectors, position and readout behavior. Physics generator used for simulation produced only elastic pp scattering process at energy $\sqrt{s} = 200 GeV$.

160 Kinematic range covered uniformly azimuth angle $-\pi \leq \phi \leq \pi$ and four-momentum transfer t within the range $0.01 \leq |t| \leq 0.5$ (GeV/c)² distributed as $dN/dt \sim \exp(-B \cdot t)$ with $B = 14$ (GeV/c)⁻².

5.1. Efficiency

The detector geometrical acceptance and limited aperture of the DX magnet require that reconstructed distribution of four-momentum transfer t is corrected. Differential distribution $(dN/dt)^{DATA}$ obtained from data was corrected using “bin by bin” method (a diagonal method) with correction factors obtained through Monte Carlo simulation according with formula 2.

$$\left(\frac{dN}{dt}\right)_{corrected}^{DATA} = \left(\frac{dN}{dt}\right)_{reconstructed}^{DATA} \times \frac{(dN/dt)_{generated}^{MC}}{(dN/dt)_{reconstructed}^{MC}} \quad (2)$$

170 here $(dN/dt)_{generated}^{MC}$ and $(dN/dt)_{reconstructed}^{MC}$ are true MC distribution and reconstructed based on MC event sample which passed reconstruction and selection steps identical as those applied for experimental data.

5.2. Beam Tilt

Given unknown beam position and direction relative to detector coordinate system, the detector response correction function:

$$R(t_{rec}, t_{gen}) = \frac{(dN/dt)_{gen}^{gen}}{(dN/dt)_{rec}^{rec}} \quad (3)$$

175 was obtained from MC simulation with beam trajectory parallel to detector local coordinate z-axis. In the actual detector setup a tilt of beam axis and detector z-axis may be present, and alignment procedure is not capable to correct for. Tilt causes an offsets τ_x and τ_y of reconstructed θ_x and θ_y angles, this leads to offset of calculated four-momentum transfer \mathbf{t} :

$$\Delta \mathbf{t} \simeq 2 \cdot p^2 \cdot (\theta_x \cdot \tau_x + \theta_y \cdot \tau_y) \quad (4)$$

180 (here terms τ_x^2 and τ_y^2 were neglected).

Presence of tilt makes MC simulated correction function inaccurate and the fit of corrected (dN/dt) distribution with expected $A \cdot \exp(-B \cdot t)$ is poor. An

iterative approach is made to improve fit quality by adding several values of τ_x, τ_y to reconstructed values of θ_x, θ_y and seeking for best fit probability. It is achieved for $\tau_x \approx 0.15 \cdot 10^{-3} rad$. We observe a weak dependence of the fit results, slope \mathbf{B} and total cross-section σ_{tot} on tilts values.

6. Results

The four-momentum transfer squared t was calculated $-t = p^2 \cdot (\theta_x^2 + \theta_y^2)$, where θ_x and θ_y are calculated by fitting a straight line using four track point events, two on each side of the IP. The corrected for efficiency t distribution is shown in Fig. 4

The evaluation of the systematic uncertainties due to the uncertainty in beam emittance, vertex positions and its spread, and incoming beam angles was based on Monte Carlo simulations. These simulations used the geometry of the experimental setup and efficiency of the detectors as an input. The largest single source of the systematic error was the uncertainty of the initial colliding beam angles (the beam tilt angle).

This possible shift of the t -distribution scale was studied with the Monte Carlo simulation, using upper limits on the beam tilt angle obtained from data. This resulted in an uncertainty on the fitted slope parameter of about 2%.

Another systematic uncertainty is due to luminosity determination and estimated to be 7%, relative. This is scale uncertainty on the vertical scale of the cross section plot. Hence it does not affect the value of the slope parameter B , but introduces a corresponding systematic uncertainty on the measured cross sections: σ_{tot} , $\sigma_{elastic}$ and $\frac{d\sigma}{dt}$.

The GEANT4 simulation, which includes background contribution from the scattered protons interacting with the material in front of the Roman Pots, like the beam pipe, magnet structure and RF shield inside the DX-D0 chamber. The estimated background contribution within the geometrical acceptance is 0.4%.

210 **7. Summary**

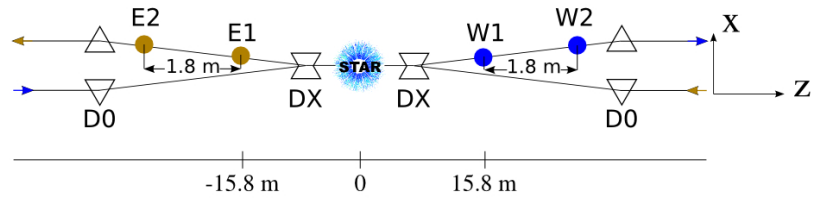
At $\sqrt{s} = 200$ GeV at RHIC the STAR experiment measured differential cross-section of elastic proton-proton scattering as a function of t in range $0.045 < -t < 0.125$ GeV^2 . Differential elastic cross-section is well described by exponential fit with the slope $B = 14.2 \pm 0.1(\pm 0.3)$ GeV^{-2} , in brackets systematic uncertainty is quoted. Extrapolation of measured differential elastic cross-section over non-detected ($\approx 40\%$) low t region allowed to determine elastic cross-section to be $9.6 \pm 0.1(\pm 0.7)$ mb, and using optical theorem total pp cross-section was found to be $51.3 \pm 0.4(\begin{smallmatrix} +2.1 \\ -1.9 \end{smallmatrix})$ mb. The asymmetric systematic uncertainty is due to the luminosity uncertainty, which is the dominant uncertainty of the measurement. We find that the obtained results compare well with the world data as summarized in[5].

References

- [1] Models here
- [2] S. Bültmann *et al.*, Nucl. Instr. Meth. **A535**, 415 (2004).
- 225 [3] R. Sikora these proceedings and arXiv: <https://arxiv.org/abs/1811.03315>
- [4] L. Fulek these proceedings.
- [5] G. Antchev et al.,TOTEM Experiment, arXiv:1712.06153v2 [hep-ex] and references there in.

Figures

Top view



Side view

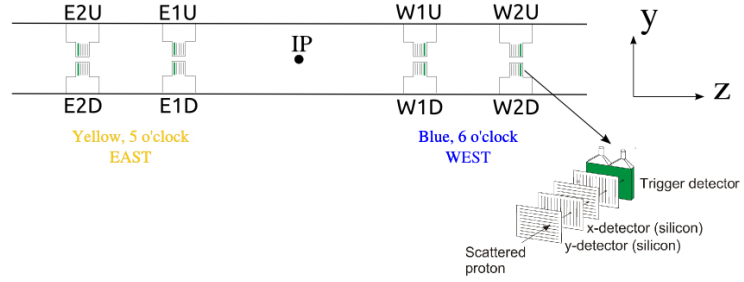


Figure 1: The layout of the experiment.

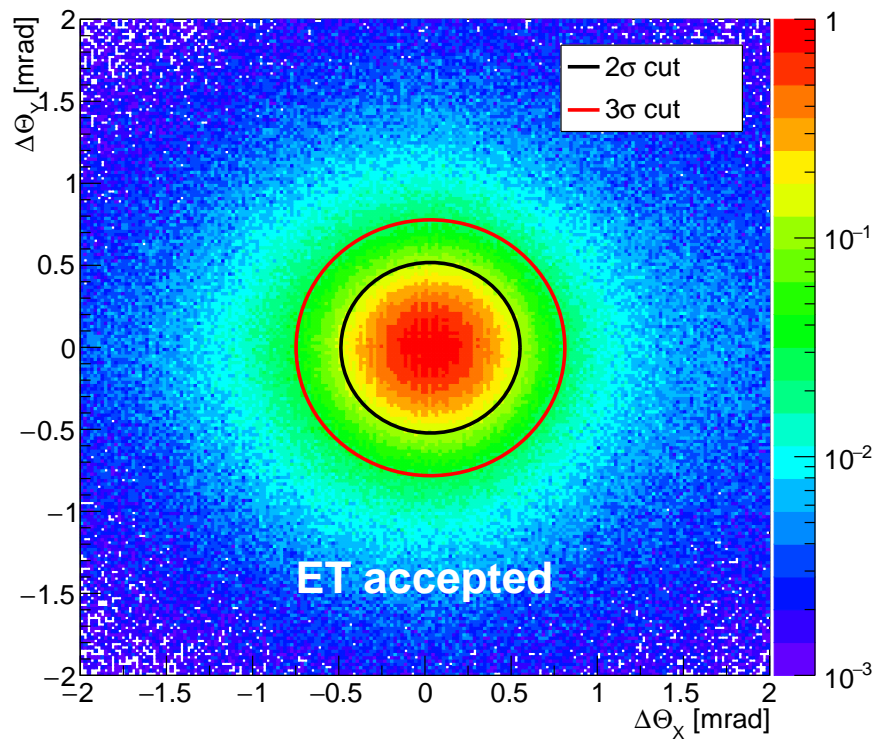


Figure 2: $\Delta\theta_y$ vs $\Delta\theta_x$ with the contours of 2σ and 3σ .

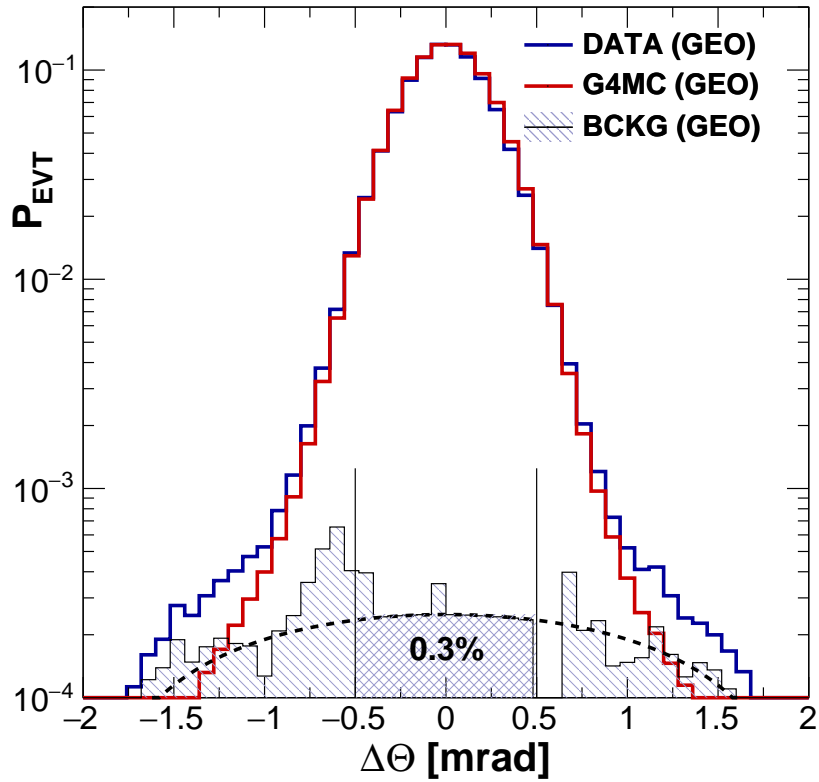


Figure 3: Co-linearity $\theta_{west} - \theta_{east}$ data compared with G4MC (pure elastic scattering events only) simulated distributions. Estimated background, hatched area, and background remained after co-linearity cut (hatched rectangles) are shown.

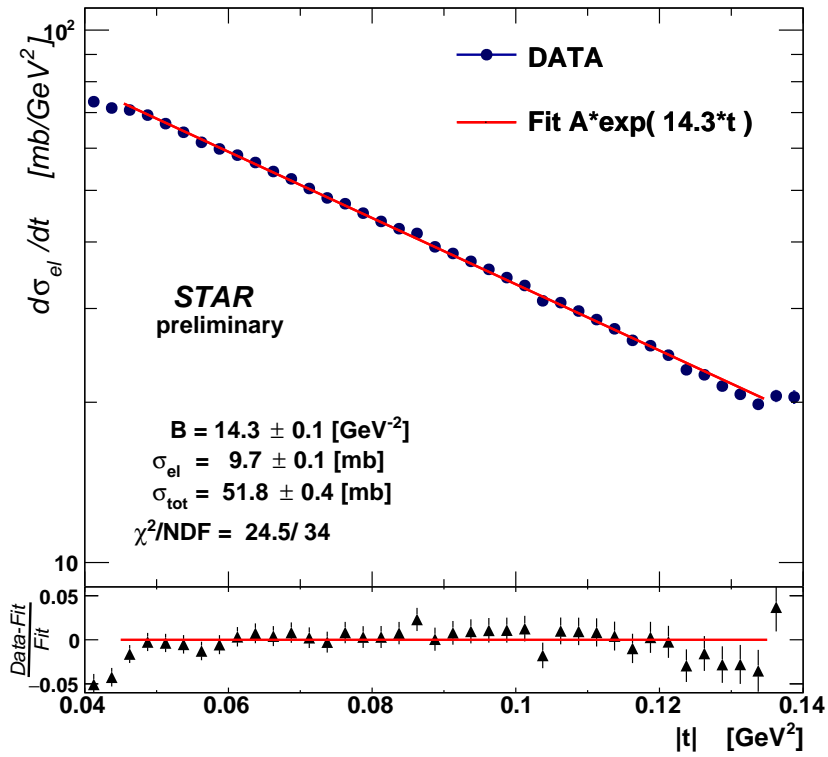


Figure 4: Corrected differential cross-section dN/dt fitted with exponential $A \cdot \exp(-Bt)$.

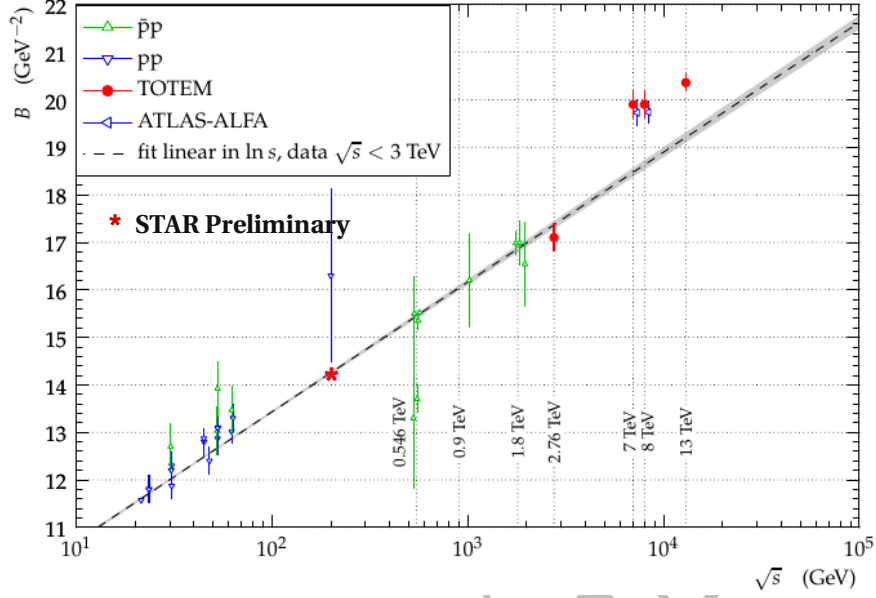


Figure 5: Comparison of STAR result on B-slope with the world data.

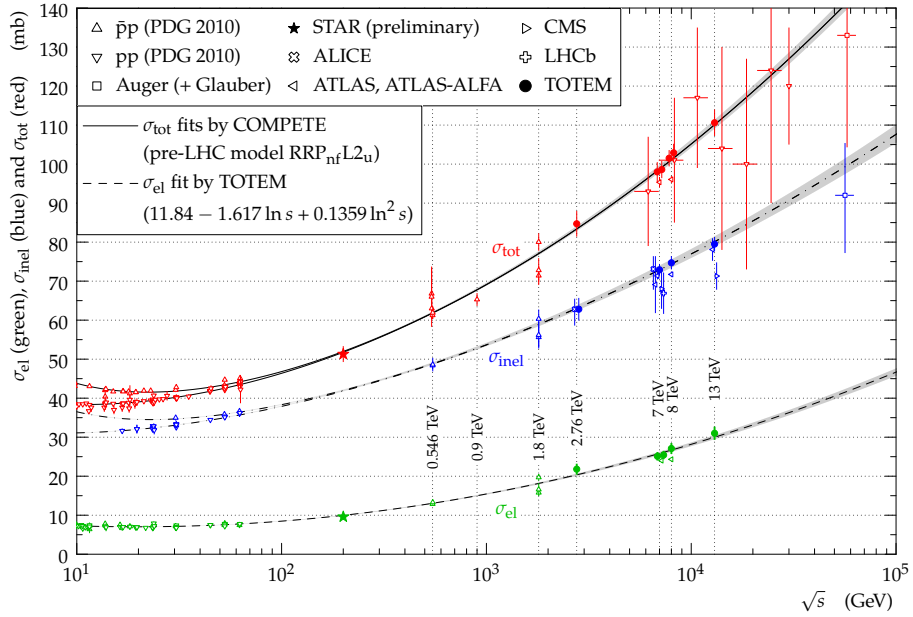


Figure 6: Comparison of STAR result on σ_{el} and σ_{tot} with the world data.

Table 1: Result summary with systematic uncertainties contributions.

Quantity			Statistical uncertainty	Systematic uncertainties				
name	units	Value		$ t - dep$	norm	lumi	ρ	full
$d\sigma_{el} / dt_{t=0}$	[mb/ GeV ²]	137.1	± 1.1	2.4	0.6	$^{+10.2}_{-8.9}$	n/a	$^{+10.5}_{-9.3}$
B	[GeV ⁻²]	14.3	± 0.1	0.3	n/a	n/a	n/a	± 0.3
σ_{el}	[mb]	9.7	± 0.1	0.1	0.04	$^{+0.7}_{-0.6}$	n/a	± 0.7
σ_{tot}	[mb]	51.8	± 0.4	0.5	0.5	$^{+1.9}_{-1.7}$	$^{+0.2}_{-0.4}$	$^{+2.1}_{-1.9}$